

Diameter-Dependent Shape Memory Effect and Superelasticity in Ni-Mn-Ga Alloy Micro-fibers

Guanhua Zhang¹, Jiayue Xu¹, Haoyang Xie¹, Zihan Yang¹, Yan Feng^{2,*}, Mingfang Qian³ and Jianfei Sun^{3,*}

¹Queen Mary University of London Engineering School, Northwestern Polytechnical University, Xi'an 710100, China

²School of Materials Science and Engineering, Northwestern Polytechnical University, Xi'an 710129, China

³School of Materials Science and Engineering, Harbin Institute of Technology, Harbin 150001, China

Abstract: The functional properties of shape memory alloys (SMAs) may be affected by the material size and thus is important for designing micron-sized devices. Here the diameter-dependent size effect was demonstrated in Ni-Mn-Ga fibers with diameters of 15, 41, 53 and 70 μm . The effect of fiber diameter on the shape memory effect (SME) and superelasticity (SE) was systematically studied. The results showed that all Ni-Mn-Ga fibers exhibited good stress assisted thermal cycles and SE, both diameter-dependent. For stress assisted thermal cycles, the temperature hysteresis of martensite transformation (MT) and sensitivity of MT temperature vs stress increased with increasing fiber diameter. While for SE, the stress hysteresis, temperature dependence of critical stress and energy dissipation capacity decreased with increasing fiber diameter. Thermodynamic analysis revealed that the diameter-dependent effect may be attributed to the different heat exchange and frictional work dissipation capacities related to the specific surface areas that affected the thermal- or stress-induced MT processes. Such diameter dependence in Ni-Mn-Ga micro-fibers needs to be considered for the design and application in micro-sized devices.

Keywords: Stress assisted thermal cycles, Superelasticity (SE), Martensite transformation (MT), Size effect, Ni-Mn-Ga micro-fiber.

1. INTRODUCTION

Microelectromechanical systems (MEMS) require small-sized sensors and actuators for applications in various fields [1-3]. The development of multifunctional smart materials and related miniaturization technology has created a new generation of smart micron-sized MEMS devices [4]. Among these smart materials, shape memory alloys (SMAs) have attracted wide attention because of high output power density, good shape memory effect (SME) and superelasticity (SE) [5-8]. In particular, MEMS devices integrated with micron-sized SMAs may exhibit special properties for potential applications in new highly compact precise sensors, actuators, shock absorbers and energy conversion devices. It is well known that the functional properties, such as SME and SE, are closely related to the martensite transformation (MT) induced by external temperature change or stress. Consequently, a systematic study on the size effect of MT in SMAs may play an important role in the design of micron-sized devices [9].

In this work, an in-depth study was conducted on the diameter dependence of stress assisted thermal

cycles and SE in Ni-Mn-Ga alloy micro-fibers. Ni-Mn-Ga alloys belong to a kind of ferromagnetic shape memory material [10, 11], which can be driven by temperature change or a magnetic field. Compared with traditional SMAs, Ni-Mn-Ga alloys showed the advantages of very fast response speed and high efficiency under a rotating magnetic field [12-16]. Small-sized Ni-Mn-Ga alloys, such as micro-fibers, exhibit application prospects in many smart micro-devices in MEMS systems. However, there is a lack of systematic study on the phenomenon and mechanism of size effect in Ni-Mn-Ga fibers. Here, this work focused on the stress assisted thermal cycles and SE properties of Ni-Mn-Ga fibers with diameters $\Phi 15\text{-}70 \mu\text{m}$ prepared by melt-spinning [17]. The diameter dependence of stress assisted thermal cycles and SE in Ni-Mn-Ga micro-fibers was demonstrated and may be explained by the different heat exchange and frictional work dissipation capacities related to the difference specific surface areas based on the thermodynamic analysis. The results may help in the design of Ni-Mn-Ga fibers in micron-sized devices.

2. MATERIALS AND METHODS

Ni-Mn-Ga master alloy ingots with composition of $\text{Ni}_{50.3}\text{Mn}_{26.9}\text{Ga}_{22.8}$ (data indicate mass percent, wt.%) were prepared by vacuum arc melting and casting into

*Address correspondence to this author at School of Materials Science and Engineering, Northwestern Polytechnical University, Xi'an 710129, China; E-mail: yanfeng@nwpu.edu.cn; jfsun_hit@163.com.

copper mold. The ingots were repeatedly melted five times before casting to ensure the homogeneity of the composition. Ni-Mn-Ga micro-fibers were prepared by a melt-spinning technique, during which different diameter fibers were obtained by adjusting the feeding rate of the parent ingot and the spinning speed. The obtained fibers usually exhibited a fairly wide-range of diameter distribution. In this work, only four kinds of fibers with smooth surface and diameter $\Phi 15$, 41, 53 and 70 μm (named as D15, D41, D53 and D70, respectively) were selected to study the stress assisted thermal cycles and SE.

The stress assisted thermal cycles and SE tests were conducted on a dynamic mechanical thermal analyzer (DMA, Netzsch 442E) using a tensile mode. The length of the tensile specimens has a length of 10mm. The stress assisted thermal cycles were carried out at a temperature range $-10\sim 80^\circ\text{C}$ under various loads (see Table 1). The heating and cooling rates during cycles were $5^\circ\text{C}/\text{min}$. The SE test was carried out at temperatures above the martensite starting temperature (M_s) under various bia-stresses. During SE cycle, the loading rate was 0.02 N/min while the

unloading rate was 0.04 N/min. Details of the experimental parameters are listed in Table 1.

3. RESULTS

3.1. Stress Assisted Thermal Cycles in Ni-Mn-Ga Fibers

Figure 1 shows the stress assisted thermal cycles of Ni-Mn-Ga fibers with diameters 53 μm (D53) and 41 μm (D41) under a temperature range $-10\sim 80^\circ\text{C}$ and loads 0.1-0.35 N. The cyclic curves of D53 fiber under different loads are shown in Figure 1a. As the load increases, the maximum strain and MT critical temperatures increase. At the same time, the residual strain increases with increasing load, which is related to occurrence of irreversible defects (e.g. dislocations or stabilized residual martensite) during multiple cycles. On the other hand, the defects generated at low stress can provide martensite nucleation sites for subsequent MT at high stress, also inducing the right shift of transformation temperatures (*i.e.* stabilization of parent phase) [18].

Figure 1b shows nine cyclic curves of D41 under load 0.15 N (68 MPa). With increasing cycles, the

Table 1: Stress Assisted Thermal Cycles and Superelastic (SE) Test Parameters in $\text{Ni}_{50.3}\text{Mn}_{26.9}\text{Ga}_{22.8}$ Micro-Fibers with Different Diameters (^a Single-Cycle; ^b Multiple Cycles)

Diameter (μm)	Stress Assisted Thermal Cycles Test Load (N)	SE Test Temperature ($^\circ\text{C}$)
15 (D15)	0.1, 0.2, 0.5 ^a	28, 30, 32, 35
41 (D41)	0.15 ^b	—
53 (D53)	0.1, 0.15, 0.2, 0.25, 0.3, 0.35 ^a	28, 30, 32, 35, 37, 40, 42
70 (D70)	0.05, 0.2 ^a	30, 32, 35, 38

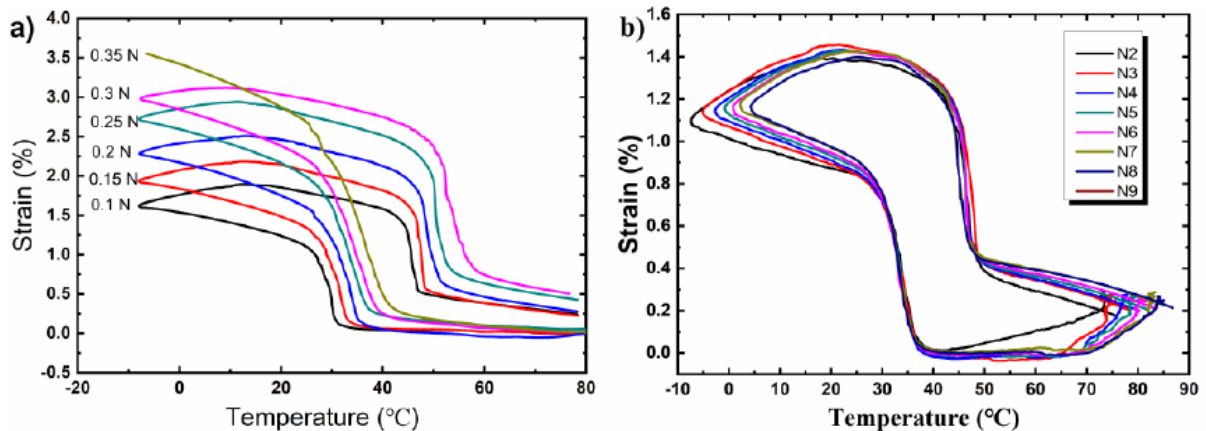


Figure 1: Stress assisted thermal cycles of Ni-Mn-Ga fibers with different diameters. (a) D53 under loads of 0.1-0.35 N, (b) D41 under load of 0.15N.

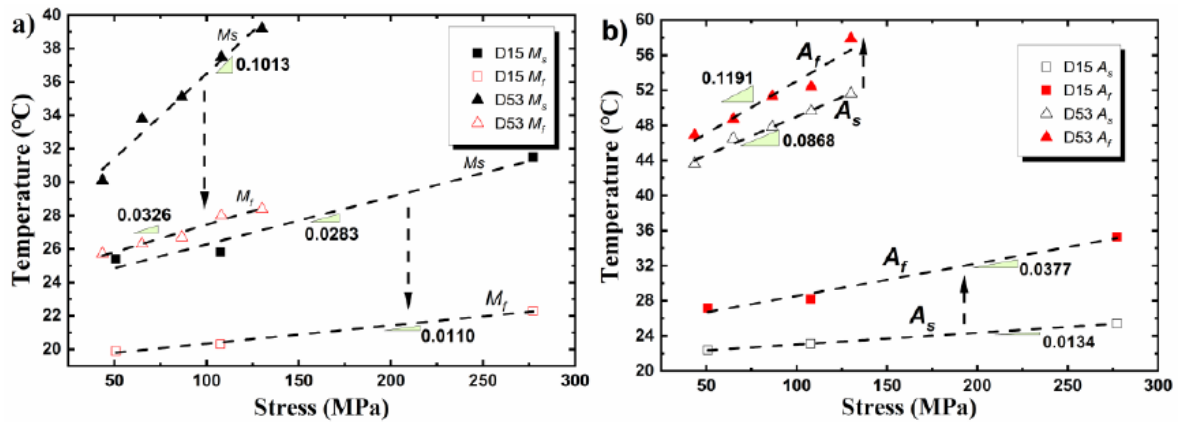


Figure 2: Linear fitting plots of MT temperatures in fibers D15 and D53. (a) M_s , M_r ; (b) A_s , A_r .

transformation temperatures remain almost unchanged; that is to say, the fiber exhibits a stable stress assisted MT behavior during multiple cycles.

The MT temperatures (M_s , M_r , A_s , A_r), and temperature hysteresis (ΔT) obtained from the stress assisted thermal cycles were statistically analyzed. Figure 2 shows the linear relationship between MT temperatures and external stress in fibers D15 and D53. The MT temperatures show a linear relationship with stress, which follows the Clausius–Clapeyron (C-C) relation. The sensitivity of MT temperatures to stress can be represented by the slope of the fitted C-C plots. As shown in Figure 2a, the slope of the M_s and M_r of D15 is 0.0283 and 0.0110 °C/MPa, respectively, while that of D53 is 0.1013 and 0.0326 °C/MPa, respectively. Similar trend also happens for A_s and A_r in D15 and D53 fibers, as shown in Figure 2b. Obviously, the sensitivity of MT temperatures to stress (*i.e.* the slope of the C-C curves) in D15 fiber is smaller than that of D53 fiber.

The MT hysteresis is defined as the difference between A_s and M_r , *i.e.* $\Delta T = A_s - M_r$. The larger the hysteresis during MT, the larger the driving force required for MT. When defects such as dislocations are produced during MT, the hysteresis tends to increase. Figure 3 shows the stress dependent ΔT of fibers with different diameters. The amplitude of stress variation ΔT of fibers with the same diameter is significantly smaller than that of fibers with different diameters. Obviously, the ΔT in large diameter fibers is larger than that in smaller ones. So, both MT temperature sensitivity and ΔT of fine fibers are smaller than those of larger diameter fibers, confirming the diameter dependence in Ni-Mn-Ga micron fibers.

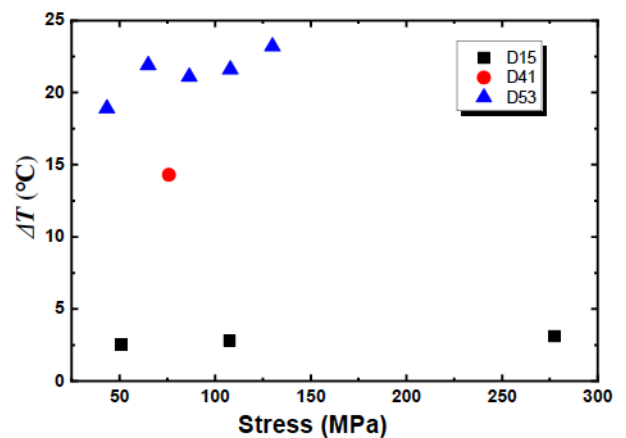


Figure 3: MT hysteresis (ΔT) as a function of external stress during stress assisted thermal cycles in fibers D15, D41 and D53.

3.2. SE in Ni-Mn-Ga Fibers

Figure 4 shows the superelastic curve of D15 fiber. Figure 4a shows the SE curves at different temperatures. The critical superelastic plateau stress increases with increasing temperature. In addition, the recoverable strain during unloading process is higher at high temperature, *e.g.* the residual strain decreases from 0.75% at 28 °C to about zero at 35 °C. The stress hysteresis also decreases with increasing temperature. The reason for such temperature dependence may be attributed to accumulated elastic energy during stress induced martensite transition (SIMT), which acts as the driving force for strain recovery. However, the storage elastic energy is not enough to fully recover the strain when the temperature is too low, which produces some residual strain. At high enough temperatures, the storage elastic energy may promote full strain recovery, resulting in a decrease in residual strain and stress hysteresis [19, 20].

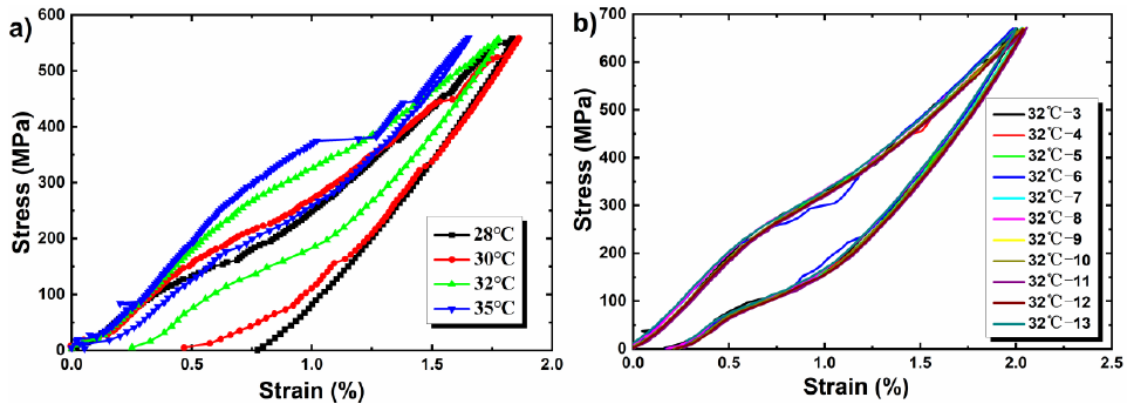


Figure 4: Superelastic (SE) curve of fiber D15. (a) SE curves at different temperatures; (b) 10 consecutive SE cycles at temperature 32°C (1st and 2^{ed} plots not shown here as they are unstable).

Figure 4b shows the superelastic cycle curve for 10 consecutive cycles at 32°C. It is noted that the superelastic curves gradually stabilize after multiple cycles. In addition, the SE stress remains basically unchanged, indicating that repeated cycles can improve the stability of the SE behavior.

The abovementioned results clearly imply that the SE stress and stress hysteresis exhibit size dependence. Figure 5 shows the linear fitting plots of SE critical stress as a function of temperature in D15, D53 and D70 fibers. As expected, the SE stresses increase linearly with temperature, where the slope ($d\sigma/dT$) represents the sensitivity of SE stresses to temperature. It is noted that, the temperature dependent SE stresses decreases with the increase of fiber diameter in different diameter fibers of D15, D53 and D70. From the extrapolation of the linear relationship curves, the MT temperatures can be obtained. For example, the M_s of D15 and D53 fibers are 23.3°C and 26.7°C respectively, which is consistent with the results obtained from the stress assisted thermal cycles.

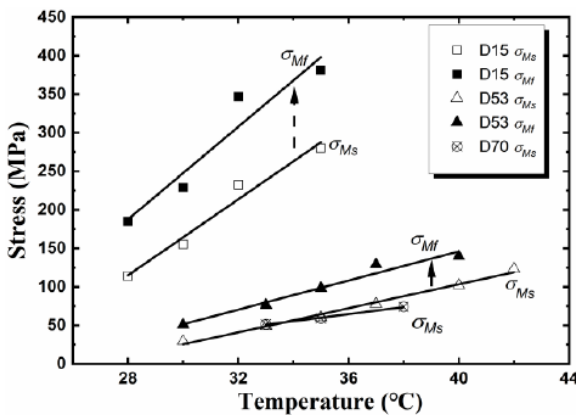


Figure 5: Linear fitting plots of SE stress as a function of temperature in fibers D15, D3 and D70.

The stress hysteresis ($\Delta\sigma$) during SE process obtained at different temperatures in D15 and D53 fibers is displayed in Figure 6. It can be seen that the $\Delta\sigma$ in D15 is 55-60 MPa, much larger than that of D53 fiber (20~23 MPa). In addition, the change of hysteresis with temperature is very small for each fiber.

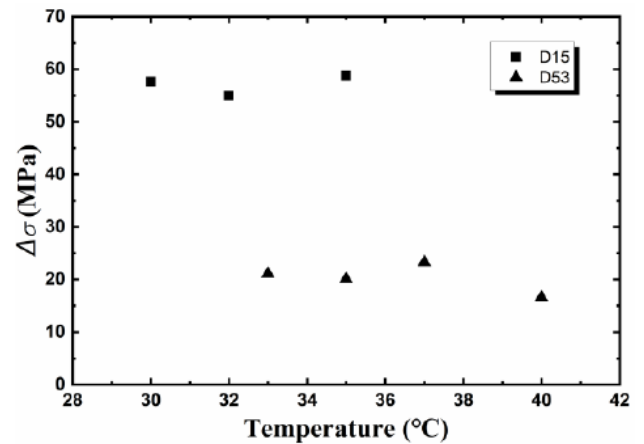


Figure 6: Temperature dependent SE stress hysteresis ($\Delta\sigma$) in fibers D15 and D53.

The energy dissipation of SMAs is closely related to the critical stress and $\Delta\sigma$ during SE process [21]. Here, $\Delta E_{1\%}$ is defined as the energy dissipation of 1% strain per unit volume in SE cycle. Considering the difference of MT temperatures, only the data of superelastic temperatures more than 10°C away from the transformation temperature are analyzed. The $\Delta E_{1\%}$ of D15, D53 and D70 fibers are analyzed and the results are shown in Figure 7. It can be seen that $\Delta E_{1\%}$ in fibers with different diameters all exhibit a linear dependence on temperature. In addition, $\Delta E_{1\%}$ decreases with increasing temperature, but showing different rates in different diameter fibers. The sensitivity of $\Delta E_{1\%}$ to temperature can be expressed by

the slope of the fitted straight line $d\Delta E_{1\%}/dT$. Among them, the $d\Delta E_{1\%}/dT$ of D15 fiber is the largest ($-9.48 \times 10^4 \text{ J/m}^3$), followed by D53 ($-4.22 \times 10^4 \text{ J/m}^3$), and that of D70 ($-3.17 \times 10^4 \text{ J/m}^3$) is the smallest. Obviously, the $d\Delta E_{1\%}/dT$ of fibers is diameter-dependent.

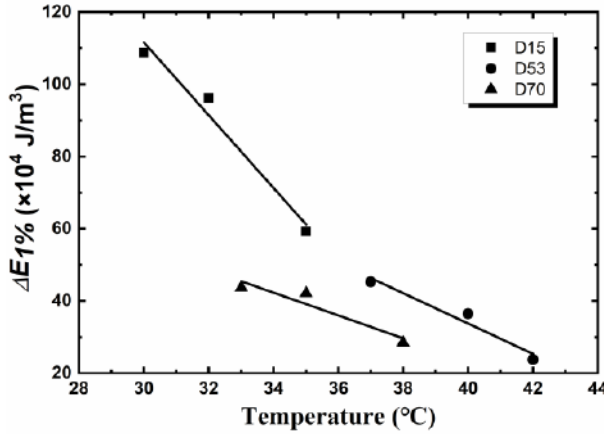


Figure 7: $\Delta E_{1\%}$ and linear fitting diagram in fibers D15, D53 and D70.

4. DISCUSSIONS

4.1. Diameter Dependence of MT in Ni-Mn-Ga Fibers

The driving forces of MT mainly include chemical and non-chemical free energy. The non-chemical free energy mainly consists of interface energy, surface energy, elastic storage energy, etc. According to ref. [22], the rate of Gibbs free energy during MT of a sample under stress can be described as:

$$\dot{G} = [\Delta G_{ch} + \tilde{\alpha} A_i + \tilde{\alpha}_{st} A_{sf} + E_{el}] \dot{f} + E_{fr} \left| \dot{f} \right| - \dot{\sigma} \dot{\epsilon} \quad (1)$$

During forward MT, the strain rate in the positive transformation $\dot{\epsilon} > 0$ and the change rate of martensite volume fraction $\dot{f} > 0$. While during backward MT, $\dot{f} < 0$ and $\dot{\epsilon} < 0$. $\Delta G_{ch} = G_{ch}^M - G_{ch}^A = \Delta H - T\Delta S$ is the change in chemical free energy per unit volume at temperature T . When $T > A_f$ and no stress is applied, the austenite state is more stable $\Delta G_{ch} > 0$. $\tilde{\alpha}$ is the interface energy per unit area, and A_i is the interface density. $\Delta \gamma_{sf} = \gamma_{sf}^M - \gamma_{sf}^A$ is the surface energy difference between martensite and austenite per unit area, and A_{sf} is the specific surface area of the fiber. E_{el} is the increment of elastic energy per unit volume during MT process. E_{fr} is an irreversible change in free energy, usually considered as the energy dissipation driving the interface in the form of frictional work. Most of E_{fr} is dissipated by thermal energy, while a very small portion is dissipated in the

form of sound waves. Obviously, the chemical energy, interfacial energy, surface energy and elastic storage energy increase with increasing content of martensite phase during forward MT, and recover with the decrease content of martensite phase during reverse transformation.

For fibers with different diameters, the grain boundary energy and elastic storage energy per unit volume are basically the same, but the surface energy per unit volume is much different. The smaller the diameter, the higher the specific surface area of the fiber. Due to the relatively small latent heat of MT, the contribution of surface energy can be ignored. However, the free surface can provide a large number of defects and pinning points for interface movement during MT process.

For multiple stress assisted thermal cycles, the forward and reverse MT are temperature induced. As a result, the heat transfer capacity [22] is an important factor affecting the MT process of SMAs because frictional work is mainly dissipated in the form of heat and also because the first-order MT process can release and absorb the latent heat via heat transfer in the inner part of a fiber. The calculation formula for the Biot number during heat transfer of a Ni-Mn-Ga fiber with a diameter (D) can be described as:

$$B_i = hL_c / k = Dh / 4k \quad (2)$$

In Equation (2), $L_c = D/4$ is the ratio of volume to surface of a fiber, thermal conductivity $k \approx 90 \text{ W/(mK)}$, and convection heat transfer coefficient $h \approx 10 \text{ W/(m}^2\text{K)}$. As the fiber diameter is on the micrometer scale (10^{-6} m), the B_i of all samples are extremely small, indicating that the heat transfer in fibers of different sizes is extremely fast relative to the convective heat transfer on the surface. Therefore, the temperature in the fibers may be considered the same, and heat transfer is mainly limited by the convective heat transfer on the surface. Therefore, it is necessary to consider the size dependence of thermal energy dissipation. When a fiber undergoes MT and generates a certain amount of heat, the heat equilibration is:

$$\dot{q} - 4h(T - T_\infty) / D - \rho C_p \dot{T} = 0 \quad (3)$$

In Equation (3), q is the heat generated during MT, T_∞ is the room temperature, ρ is the fiber density, and C_p is the specific heat capacity of a fiber. A portion of

the heat generated by MT is consumed by fiber cooling and heat release into the external environment. Assuming that the rate of heat generated during MT process is constant, from $t=0$ to t_0 , the rate of heat change $q=Q_{tot}/t_0$, where t_0 represents the MT time, which is inversely proportional to the loading rate or strain rate; Q_{tot} is the total heat generated during MT process, including the latent heat and irreversible energy dissipation, in which the irreversible energy dissipation is only a small fraction of MT latent heat. Thus, the temperature of a fiber during MT process is:

$$T(t) = T_{\infty} + \frac{Q_{tot}}{\rho C_p} \cdot \frac{\tau}{t_0} [1 - \exp(-\frac{t}{\tau})] \quad (4)$$

The transfer of heat energy per unit volume varies over time is as follows:

$$Q(t) = \frac{Q_{tot}}{t_0} \{t - \tau[1 - \exp(-\frac{t}{\tau})]\} \quad (5)$$

The thermal time constant τ in Equation (4) and (5) can be defined as $\tau=D\rho C_p/4h$. The density and specific capacity of fiber is $\rho=1800 \text{ kg/m}^3$ and $C_p \approx 460 \text{ J/(kgK}^{-1})$, respectively, τ is about $2.07 \times 10^4 \text{Ds}$. For D15, D53 and D70 fibers, τ is 0.3, 1.1 and 1.5 s, respectively. Therefore, the larger the fiber diameter, the higher the thermal time constant, meaning that the rate of heat dissipation is relatively low. Similarly, the rate of heat absorption is also relatively low.

So, the finer the fiber diameter, the faster the heat exchange rate between the fiber and surrounding environment. Thus, the fiber can release or absorb heat in a more effective manner, leading to a small thermal hysteresis during MT. Therefore, the MT temperature hysteresis of D15 fiber is small, while that of D53 fiber is relatively larger. As MT is affected by both temperature and bia-stress, D53 fiber shows more sensitive to stress since the heat transfer of D53 fibers is slower compared to that of D15 (see Figure 2).

4.2. Size Effect of SE in Ni-Mn-Ga Fibers

For superelastic cycling at a certain temperature, the forward and reverse MT are induced by stress, where stress plays a leading role. According to Equation (1), the stress hysteresis follows Equation (6):

$$(\sigma^{A \rightarrow M} - \sigma^{M \rightarrow A})\epsilon_t = E_{fr}^{A \rightarrow M} + E_{fr}^{M \rightarrow A} + \int_0^1 [-(T\Delta S)^{A \rightarrow M} + (T S)^{M \rightarrow A}] df \quad (6)$$

where ϵ_t is the maximum strain in the SE process. At a constant temperature, the sum of the last two terms in Equation (6) is zero. Then equation (7) can be obtained:

$$(\sigma^{A \rightarrow M} - \sigma^{M \rightarrow A})\epsilon_t = E_{fr}^{A \rightarrow M} + E_{fr}^{M \rightarrow A} \quad (7)$$

According to Equation (7), the stress hysteresis is mainly related to the frictional work in the SE process, which is mainly dissipated by the interfacial motion. The stress hysteresis is also related to the occurrence of defects during SE. Since free surface can provide a large number of defects and pinning points for interface motion, the magnitude of SE stress hysteresis is affected by the specific surface area of free surface.

Fibers with smaller diameters exhibit a larger specific surface area, which can provide more surface defects and pinning points. Consequently, more frictional work and larger stress hysteresis can be created in D15 fiber rather than D53 fiber. Due to the combined influence of temperature and stress on SE process and the timely heat exchange in fine fibers, the $d\sigma/dT$ of D15 fiber is the maximum, while that of D70 is the minimum (see Figure 5). As the energy dissipation of frictional work is dissipated via heat exchange, the $\Delta E_{1\%}$ of smallest diameter D15 fiber has the largest decrease rate with temperature, i.e. the $d\Delta E_{1\%}/dT$ is the maximum (see Figure 7).

5. CONCLUSION

The stress assisted thermal cycles and SE of Ni-Mn-Ga micron-fibers with diameters 15, 41, 53 and 70 μm were experimentally studied and theoretically analyzed based on the thermodynamic behavior. The diameter dependent temperature hysteresis of stress assisted thermal cycles and stress hysteresis in SE processes were demonstrated. The main conclusions can be drawn as follows:

(1) Ni-Mn-Ga fibers with different diameters exhibited good stress assisted thermal cycles and SE. The MT temperatures increased with the increase of applied load during thermal cycles and SE. Stable MT temperatures of stress assisted thermal cycles and critical stress of SE were obtained during multiple cycles under a constant load.

(2) For stress assisted thermal cycles of fibers with different diameters, a diameter dependence of the

temperature hysteresis existed during forward and reverse MT. The temperature hysteresis and the stress sensitivity of SE temperature in D53 fiber were larger than D15 fiber since larger diameter fiber exhibited a lower heat transfer rate.

(3) For the SE of fibers with different diameters, $\Delta\sigma$, $d\sigma/dT$ and $d\Delta E_{1\%}/dT$ increased with decreasing fiber diameter because smaller diameter fibers exhibited a larger specific surface area and thus higher defects/pinning points and heat transfer capacity.

AUTHOR CONTRIBUTIONS

Conceptualization, G.H. Zhang, Y. Feng, J.F. Sun; methodology, G.H. Zhang, J.Y. Xu, Z.H. Yang, M.F. Qian; validation, G.H. Zhang, H.Y. Xie, M.F. Qian and Y. Feng; formal analysis, G.H. Zhang, Z.H. Yang, H.Y. Xie, Y. Feng; investigation, G.H. Zhang, H.Y. Xie, Z.H. Yang; data curation, G.H. Zhang, Z.H. Yang, Y. Feng; writing-original draft preparation, G.H. Zhang, Y. Feng; writing-review and editing, M.F. Qian, Y. Feng, J.F. Sun; project administration, Y. Feng and J.F. Sun. All authors have read and agreed to the published version of the manuscript.

DATA AVAILABILITY STATEMENT

The data are available from the corresponding author upon reasonable request.

CONFLICTS OF INTEREST

The authors declare no conflict of interest.

REFERENCES

- Wang J.Y.; Zhang M.L.; Wang Z.X.; Sun S.; Ning Y.; Yang X.P.; et al. An ultra-low power, small size and high precision indoor localization system based on mems ultrasonic transducer chips. *IEEE T Ultrason Ferr.* 2022, 69, 1469-77. <https://doi.org/10.1109/TUFFC.2022.3148314>
- Ganji BA.; Kheiry S.; Soleimani S. Design of small size and high sensitive less-invasive wireless blood pressure sensor using MEMS technology. *Int Circ Device Syst.* 2019, 13, 39-44. <https://doi.org/10.1049/iet-cds.2018.0013>
- Biyikli N.; Damgaci Y.; Cetiner B.A. Low-voltage small-size double-arm MEMS actuator. *Electron Lett.* 2009, 45, 354-5. <https://doi.org/10.1049/el.2009.0207>
- Cui Y.T. Thermodynamic effects and applied functions of Ni-Mn-Ga alloys. Ph.D Thesis, Chongqing University, Chongqing China, 2004.
- D'Silva G.J.; Feigenbaum H.P.; Ciocanel C. On the power and efficiency of Ni₂MnGa magnetic shape memory alloy power harvesters. *Smart Materials and Structures*, 2022, 31(7), 75013. <https://doi.org/10.1088/1361-665X/ac72da>
- Feng C.; Hu D.; Gong K.; Jiang X.; Yin J.; Cao Y.; Tang X.; Yang F.; Zhou Z.; Yu G.; Evans D.A. Thickness-dependent electronic structure modulation of ferromagnetic films on shape memory alloy substrates based on a pure strain effect. *Applied Physics Letters*, 2016, 109(21), 212401. <https://doi.org/10.1063/1.4967996>
- Barth J.; Krevet B.; Kohl M. A bistable shape memory microswitch with high energy density. *Smart Materials and Structures*, 2010, 19(S19), 94004. <https://doi.org/10.1088/0964-1726/19/9/094004>
- Reynaerts D.; Van Brussel H. Design aspects of shape memory actuators. *Mechatronics*, 1998, 8(6), 635-656. [https://doi.org/10.1016/S0957-4158\(98\)00023-3](https://doi.org/10.1016/S0957-4158(98)00023-3)
- Chen Y.; Schuh C.A. Size effects in shape memory alloy microwires. *Acta Materialia*, 2011, (59), 537-553. <https://doi.org/10.1016/j.actamat.2010.09.057>
- Castan F.J.; Nelson-Cheeseman B.; O'Handley R.C.; Ross C.A. Structure and thermomagnetic properties of polycrystalline Ni-Mn-Ga thin films. *Appl Physics*, 2003, 10(93), 8492-8494. <https://doi.org/10.1063/1.1555976>
- Sozinov A.; Lilitachev A.A.; Ianska N.; Ullakko K. Giant magnetic-field-induced strain in Ni-Mn-Ga seven-layered martensitic phase. *Appl Physics*, 2002, 80, 1746-1748. <https://doi.org/10.1063/1.1458075>
- Wu G.H.; Yu C.H.; Meng L.Q.; Chen J.L.; Yang F.M.; Qi S.R.; Zhan W.S.; Wang Z.; Zheng Y.F.; Zhao L.C. Giant magnetic-field-induced strains in Heusler alloy NiMnGa with modified composition. *Applied Physics Letters*, 1999, 75(19), 2990-2992. <https://doi.org/10.1063/1.125211>
- Pagounis E.; Chulist R.; Szczerba M.J.; Laufenberg M. Over 7% magnetic field-induced strain in a Ni-Mn-Ga five-layered martensite. *Applied Physics Letters*, 2014, 105(5), 52405. <https://doi.org/10.1063/1.4892633>
- Karaca H.E.; Karaman I.; Basaran B.; Ren Y.; Chumlyakov. Y.I.; Maier H.J. Magnetic field-induced phase transformation in NiMnCoIn magnetic shape-memory alloys - A new actuation mechanism with large work output. *Advanced Functional Materials*, 2009, 19(7), 983-998. <https://doi.org/10.1002/adfm.200801322>
- Soderberg O, Ge Y, Sozinov A, Hannula S.P, Lindroos V.K. Recent breakthrough development of the magnetic shape memory effect in Ni-Mn-Ga alloys. *Smart Materials and Structures*, 2005, 14(5), s223-235. <https://doi.org/10.1088/0964-1726/14/5/009>
- Sun G.F.; Qiang W.J. Magnetic functional materials. Beijing: Chemical Industry Press, 2003, 197.
- Gonzalez J.; Ardanuy M.; Gonzalez M.; Rodriguez R.; Jovancic P. Polyurethane shape memory filament yarns: Melt spinning, carbon-based reinforcement, and characterization. *Text Res J.* 2023, 93, 957-70. <https://doi.org/10.1177/00405175221114165>
- Ueland S.M.; Schuh C.A. Superelasticity and fatigue in oligocrystalline shape memory alloy microwires. *Acta Mater.* 2012, 60, 282-292. <https://doi.org/10.1016/j.actamat.2011.09.054>
- Bechtold C.; Gerber A.; Wuttig M.; Quandt E. Magnetoelastic hysteresis in 5M NiMnGa single crystals. *Scripta Materialia*, 2008, 58(11), 1022-1024. <https://doi.org/10.1016/j.scriptamat.2008.01.035>
- Hamilton R.F.; Dilibal S.; Sehitoğlu H.; Maier H.J. Underlying mechanism of dual hysteresis in NiMnGa single crystals. *Materials Science and Engineering A*, 2011, 528(3), 1877-1881. <https://doi.org/10.1016/j.msea.2010.10.042>
- He Y. Interface propagation and energy dissipation in Shape Memory Alloys. *Scripta Mater.* 2023, 230, 115420. <https://doi.org/10.1016/j.scriptamat.2023.115420>

- [22] Zhao L.C.; Cai W.; Zheng Y.F. In Shape memory effect and superelasticity of alloys; National Defense Industry Press: Beijing, China, 2002, pp. 2-12.

Received on 11-07-2023

Accepted on 16-08-2023

Published on 24-08-2023

DOI: <https://doi.org/10.31875/2410-2199.2023.10.05>

© 2023 Zhang *et al.*; Zeal Press.

This is an open access article licensed under the terms of the Creative Commons Attribution License (<http://creativecommons.org/licenses/by/4.0/>) which permits unrestricted use, distribution and reproduction in any medium, provided the work is properly cited.